Organic Nanoscrolls from Electrostatic Interactions between Peptides and Lipids: Assembly Steps and Structure

Pierre Chervy, Cristina Petcut, Damien Rault, Cristelle Mériadec, Thomas Bizien, Keinny François, Joël Richard, Christophe Chassaing, Naziha Benamar, Franck Artzner, et al.

Organic Nanoscrolls from electrostatic interactions between peptides and lipids: assembly steps and structure.

Pierre Chervy[a,c], Cristina Petcut[a,c], Damien. Rault[b,c], Cristelle Meriadec[b], Thomas Bizien[d], Keinny François[a], Joel Richard[c]†, Christophe Chassaing[c], Naziha Benamar[c], Franck Artzner[b] & Maïté Paternostre[a*]

[a]I2BC, Institute for Integrative Biology of the Cell (I2BC), CEA, CNRS, Univ. Paris-Sud, Université Paris-Saclay, 91198, Gif-sur-Yvette cedex, France; [b]IPR, Université Rennes 1, 35000 Rennes, France ; [c]Ipsen, 28100 Dreux, France ; [d]Synchrotron Soleil, L'Orme des Merisiers, 91190 Saint-Aubin

KEYWORDS : self-assembly, peptides, lipids, electrostatic interactions.

ABSTRACT: An important aspect of cells is their shape flexibility that gives them motion but also a high adaptation versatility to their environment. This shape versatility is mediated by different types of protein-membrane interaction among which electrostatic plays an important role. In the present work we examined the interaction between a small di-cationic peptide that possess self-assembly properties and lipid model membranes. The peptide, Lanreotide, spontaneously forms nanotubes in water that have a strictly uniform diameter. In the current work, we show that the interaction between the cationic peptide and negatively charged bilayers of lipids induces the formation of myelin sheath like structures that we called nanoscrolls. By deciphering the different steps of formation and the molecular structure of the self-assembly, we show how electrostatics modify the spontaneous peptide and lipid way of packing.

INTRODUCTION

Self-assembled architectures are omnipresent in nature. Membranes, microtubules and microfilaments, chromatin, etc. are all dynamic and functional architectures playing a crucial role in the compartmentation of cellular functions. These functional and versatile materials have been selected by evolution and the chemical and physicochemical

rules governing their formation are still to be understood in detail. This is of great importance not only in biology but also for material science as the understanding of the strategies selected by nature could be used to build de novo materials with versatile properties.[1–9] Furthermore, particular attention is devoted to protein assemblies since fibrillary architectures formed by misfolded proteins have been associated to diseases in particular neurodegenerative[10] but also systemic amyloidose.[11]

In Alzheimer's disease, the amyloid β peptide is cleaved from a native membrane protein and one of the important questions is "how the membrane proximity influences this peptide self-assembly process".[12] Another example is the α-synuclein that is found concentrated in abnormal deposition of cellular material, *i.e*. Lewy bodies in some cases of hereditary Parkinson's disease.[13] This protein that forms fibers is also known to interact with membranes and to play a role in the preservation of the pool of synaptic vesicles within the neuron.[14]

On another hand, in material science, biological molecules and molecular self-assemblies are promising templates to organize well-defined inorganic nanostructures. For example, DNA-cationic membrane complexes, maintained by strong electrostatic interactions allowed the alignment of the CdS (002) polar planes parallel to the negatively charged sugar-phosphate DNA backbone, suggesting that molecular details of the DNA molecule have been replicated onto the inorganic crystal structure.[15,16] Hierarchical self-assembly of quantum dots has been realized by using a self-assembled three-dimensional crystal template of helical actin protein filaments and lipids bilayers.[17] More recently, multilamellar nanocomposite membranes composed of phospholipid multilayers and silicon nanoparticles sandwiched between each adjacent lipid layers was fabricated. In these ordered composite material, the silicon nanoparticles achieved different photoluminescence properties compared to the nanoparticles in suspension.[18]

Therefore, understanding the influence of membranes on protein self-assembly is important not only for biology and medicine but also for material science.

In the present work, we studied the interaction between lanreotide and lipid membranes. Lanreotide, an oligo peptide of eight amino acids, is a therapeutic analog of somatostatin hormone (Figure 1D). Lanreotide kept from the natural peptide hormone the self-assembly properties.[19,20] However, if somatostatin forms reversible polydispersed amyloid structures, lanreotide forms very well defined nanotubes (Figure 1 A, B & C) with a strictly uniform diameter that is essentially controlled by the close contacts between molecules within the crystalline wall of the nanotubes (Figure 1 D, E & F). This crystalline nanotube wall is formed by a bilayer of peptide. This bilayer presents two hydrophilic surfaces that protects the hydrophobic residues likes D-Nal and Tyr from water. This

unique capacity of lanreotide to form very well organized self-assembly, allowed very fundamental studies for which we deciphered not only the structure[2,21,22] but also the mechanism of formation of the nanotubes[23] and the role of the counterions in this mechanism.[24,25] Lanreotide is therefore a very simple model for deciphering the molecular and physicochemical determinants driving the self-assembly processes.

In this study, we ask the question "How do lipid membranes influence the self-assembly process of lanreotide?" Indeed, in a physiological context, self-assembly processes are influenced by many different environmental parameters and in particular by the presence of membranes. In some cases, the environment can drive the assembly to another pathway resulting in the stabilization of an architecture that is less stable than the one formed in the absence of these new parameters. In the present work, we studied the interaction between lanreotide and lipid membranes containing increasing proportions of negatively charged lipids.

RESULTS AND DISCUSSION

To determine the conditions of interaction between lanreotide and lipids, we performed ultrafiltration experiments with the idea that the large self-assemblies will remain in the retentate, while the non-assembled peptide will cross the filter. Thus after centrifugation quantification of the peptide in the filtrate by UV-Visible spectroscopy (ε_m^{280nm}=12000 $cm^{-1}M^{-1}$) will give access to the concentration of the non-assembled peptide in equilibrium with the assemblies.

The capacity of such experiment to give access to the non-assembled peptide was tested on solutions of increasing lanreotide concentration. On Figure 2A, we show the results obtained after ultrafiltration on Amicon Ultra with a membrane in regenerated cellulose and a 50 KD cut off. Other ultrafiltration units were tested but showed strong peptide absorption (see Material and Methods for details and Supplementary Information, Figure SI-1).). The evolution of the peptide concentration in the filtrate describes a curve showing two distinct domains (Figure 2 A, blue points): from 0 to 17 mM, the points describe a straight line with a slope of 0.98 followed at higher concentrations by a plateau. In the first part of the curve, the slope, close to one, indicates that *i)* that the absorption of the peptide onto the filter is negligible and *ii)* all the peptide is free and not assembled. The break between this straight line and the plateau determines a critical assembly concentration (CAC) of lanreotide of 17 mM. This concentration is in very good agreement with previous determination.[21,23]

Ultrafiltration of solutions that contain lanreotide together with unilamellar liposomes composed of neutral lipids shows an evolution of lanreotide concentration in the filtrate with the initial lanreotide concentration similar in shape to the one obtained for lanreotide alone (Figure 2 A, orange points). However, the initial straight line has a lower slope (0.69 compared to 0.98) and the break between the straight line and the plateau is also lower than for the peptide alone (12,6 mM compared to 16,6 mM). This means two things: *i)* at low concentrations part of the peptide partitions between water and lipid membrane and *ii)* the critical assembly concentration of lanreotide is lowered by this interaction. Electron micrographs of the ePC-Lanreotide retentate above this new critical assembly concentration show the coexistence of liposomes and lanreotide nanotubes (Supplementary Information Figure SI-2) indicating that upon the "mixed critical assembly concentration", lanreotide self-assembles into classical nanotubes. Therefore, the interaction between neutral lipids and lanreotide indicates that lanreotide can probably cross the lipid membrane by passive diffusion and that upon a critical concentration the peptide forms regular nanotubes.

The same ultrafiltration experiments have been performed on samples containing lanreotide together with negatively charged membranes (Figure 2, panels B & C). For these experiments, we plot the evolution of the concentration of lanreotide determined in the filtrates after spinning versus the charge ratio R_q defined by the ratio between the positive charges of the peptide and the negative charges of the lipids:

$$R_q = 2*[\text{Lanreotide}]/[\text{anionic lipids}] \quad (1)$$

Table 1: Saturation charge ratio "R_q^{sat}" for membranes composed of different lipid (ePC, ePA, DMPC and DMPA) and of different negatively charged lipid proportions

$[lip]_{tot}$ mM	DMPC % M/M	DMPA % M/M	ePC % M/M	ePA % M/M	R_q^{sat}
26	90	10	-	-	1
26	50	50	-	-	0,8
26	30	70	-	-	0,9
26	30	70	-	-	0,9
10	30	70	-	-	1
10	-	-	90	10	1.4
10	-	-	30	70	1.1

This representation allows the direct comparison of the experiments performed with different lipid composition and concentrations. Contrary to neutral lipid membranes, as soon as negatively charge lipids (ePA or DMPA) are added

to the membranes, the peptide interacts strongly with the lipids as no peptide is measured in the filtrates until a R_q of 1, *i.e.* the electro neutrality (Figure 2, B & C). Moreover, independently of the proportion of negatively charged lipids in the membrane (from 10 to 70% (M/M) or the nature of negatively charged lipids (ePA or DMPA), the R_q^{sat} for saturation is close to one (Table 1). A slight difference can be seen when ePA/ePC or DMPA/DMPC mixtures of lipids are used: the R_q^{sat} for natural lipids being slightly higher than for synthetic lipids (Table 1). Above this ratio, non-assembled lanreotide is detected

Electron microscopy of DMPC/DMPA (30/70% M/M)-lanreotide mixture for R_q values of 0.5, 1 and 2 has been performed either after negative staining (Figure 3 A, B & C) or after freeze fracture (Figure 3 D & E). For negative staining, we had to dilute the samples to get observable grids. This dilution can break nanotubes of pure lanreotide as they are sensitive to concentration, but the mixed lanreotide/lipids architectures were not affected by dilution as no free peptide is in equilibrium. As soon as the peptide was added to a suspension of unilamellar liposomes, we detected the presence of different assemblies and the disappearance of liposomes. For R_q =0.5, liposomes, planar lamellae, curved lamellae and "myelin sheath type structures" that we called "nanoscrolls" coexist. For R_q =1, curved lamellae and a majority of nanoscrolls coexist and for R_q =2, only nanoscrolls are detected. The photos taken after freeze-fracture show the internal structure of these nanoscrolls that are formed by the winding of multilamellar structures (Figure 3 D). The density profiles determined using ImageJ, on different part of a multilamellar nanoscroll (Figure 3, D lower panel) give an interlamellar distance of 60±10Å. The micrographs Figure 3E show the internal structure of different nanoscrolls that can be composed of the winding of 1, 2, 3 or 4 stacked lamellae. At the center of the nanoscrolls, the deep etching reveals a water column, the internal diameter of which is about 17nm ±3 nm (average on 63 measurements) close to the internal diameter of pure peptide nanotubes (about 20 nm). The mean diameter of the nanoscrolls based on 225 measurements is centered at 118nm±26 nm. The formation of nanoscrolls is independent of the chain lengths, of the chemical nature of the head group of the anionic lipids or of the presence of complex natural lipid mixtures cells plasmic membrane (Figure SI-3). The nanoscrolls can be fitted by an Archimedean spiral (Supplementary Information, Figure SI-4) confirming that the interdistance between lamellae is constant.

These micrographs allow to draw intermediate steps of the nanoscrolls formation (Figure 4). When negatively charged unilamellar liposomes and lanreotide are mixed together, the liposomes disappear in favor of planar lamellae that curve and form either diagonal nanoscrolls (upper schemes and micrographs) or on-sided nanoscrolls (lower

scheme and micrographs). The spontaneous curvature of the multi-lamellae suggests an asymmetric structure of the assembly.

To solve the question of the molecular structure of these nanoscrolls, we performed both X-ray scattering experiments and ATR-FTIR measurements (Figure 5).

The Amide I ATR-FTIR spectrum of lanreotide gives access to the conformation of the peptide within the assemblies. A typical ATR-FTIR Amide I spectrum of nanotubes of lanreotide shows five components that were previously assigned in agreement with literature[26,27] to turn secondary structure (1664cm^{-1}) and to two different antiparallel β-sheet organizations (1620cm^{-1} and 1682cm^{-1} and 1640cm^{-1} and 1692 cm^{-1})[21] (Figure 5A). These vibrations were shown to correspond to a β-hairpin peptide backbone conformation developing an inner- and an inter-antiparallel β-sheet network. The ATR-FTIR spectra of the DMPC/DMPA (30/70% M/M) unilamellar vesicles is shown on Figure 5C. The decomposition of the peak between 1700 and 1770 cm^{-1} gives two bands that correspond to H-bounded ester (1725cm^{-1}) and unbounded ester (1742 cm^{-1}) of the glycerol backbone[28] leading to a proportion of 61% of unbounded ester and 39% of H-bounded ones. On this spectra we can also see a large band between 1600 and 1700 cm-1. This remaining band probably comes from water as we could only remove it after drying the sample on the ATR crystal using nitrogen flux. This large band that always remains after bulk water subtraction could be due to either encapsulated water within the liposomes or water in strong interaction with lipids that should both have a slightly different spectrum than bulk water. Figure 5B represents the spectra recorded for a solution that contains DMPC/DMPA and Lanreotide for an R_q of 1. The decomposition of both Amide I and ester band shows exactly the same peak positions than for peptide and lipids separately. The amide I decomposition gives the same proportions of the different structural elements than for lanreotide nanotubes and indicates that in presence of negatively charge membranes *i)* the peptide is self-assembled, *ii)* the peptide is in a β-hairpin peptide backbone conformation and *iii)* it develops an inner- and an inter-antiparallel β-sheet network very similar to the network present in the pure peptide nanotubes. Moreover, the ester band decomposition gives a proportion of unbounded and H-bounded ester only slightly different than for pure vesicle suspension, *i.e.* 36% of H-Bounded ester instead of 39% for pure lipids indicating that the peptide barely disturbed the lipid's glycerol backbone and thus did not penetrate deeply within the lipid lamellar phase. This conformational information indicate that the molecular packing of lanreotide within the nanoscrolls and within the walls of the nanotubes are very similar and that the peptide essentially interacts with the surface of the lipid bilayer.

Figure 5 (D, E and F) presents the X-ray patterns of DMPC/DMPA-lanreotide mixtures with R_q of 0.5, 1, 1.6 and 2. For reference, we also plot the patterns obtained for lipid unilamellar vesicles (Figure 5, lower black trace) and peptide nanotubes (Figure 5, upper black trace). In the small angle range (Figure 5D), the X-Ray patterns obtained for lipid-peptide evidence the absence of peptide nanotubes and of unilamellar vesicles. The intense peaks at about 0.1 and 0.2 $Å^{-1}$ indicate that the interaction between the di-cationic peptide and the anionic membranes induces a lamellar stacking with a typical interdistance of 66±1Å. This interdistance is in very good agreement with the interdistance determined from freeze fracture replica of multilamellar nanoscrolls (Figure 3). Interestingly, from R_q 0.5 to 1.6, the interlamellar distance is independent of the concentration of peptide. Other peaks are also present on the traces and will be discussed and attributed later.

In the intermediate q range (Figure 5 E), the series of peaks centered at 0.35$Å^{-1}$ is typical of the β-sheet network of the lanreotide packed in the nanotubes. These patterns show that lanreotide, even at low concentration, well below its CAC, self-assembles as soon as it interacts with the negatively charge membranes.

Finally in the wide angle region (Figure 5F), the peak detected on all the patterns reveals the organization of the lipid aliphatic chain. As a function of R_q increase, the wide angle peak *i)* decreases in intensity indicating that the interaction with increasing amount of peptide, the aliphatic chains have a tendency to melt and *ii)* changes in shape indicating that the aliphatic chains changes orientation within the bilayer. The analysis of the peak shape at R_q =1 gives a maximum angle of 40° (supplementary information, Figure SI-5).

For samples containing higher amounts of lanreotide (R_q >2) distinct macroscopic phases coexist that contain preferentially either nanoscrolls or peptide nanotubes (Supplementary Information, Figure SI-6).

The X-ray scattering patterns have been recorded as a function of temperature between 23.5°C and 55°C for different R_q (0< R_q <3.6). In Figure 6 (A, B & C) we plot the evolution of the X-Ray pattern for DMPC/DMPA (30/70% M/M) and R_q =1.2 with temperature (from 23.5 to 55°C). Membranes formed by mixtures of DMPC and DMPA present gel to fluid transition that depends on the proportion of each lipids. For membrane composed of DMPC/DMPA (30/70% M/M), we detected the transition between gel and fluid phase between 40°C and 45°C in agreement with literature[29]. At small angles, (Figure 6A), the pattern of DMPC/DMPA/lanreotide (R_q =1.2) at 23.5°C already evidences a coexistence of gel and fluid phases of lipids as seen by the higher angle shoulders of the two major Bragg peaks. With the temperature increase, the major Bragg peaks disappear in favor to a wider

angle Bragg peaks at the position of the previous shoulders. Together with the temperature induce disappearance of the wide angle peak at about 1.5Å^{-1} (Figure 6C) this evidence a gel-to-fluid lipid phase transition within the nanoscrolls. On figure 6 B, the X-Ray patterns show higher order Bragg peaks that shift with temperature but also some peaks that that remain unchanged with temperature: 0.35Å^{-1}, 0.62 Å^{-1} 0.89 Å^{-1} for the most visible. These peaks are related to the peptide packing within the nanoscrolls.

On Figure 6 D (and supplementary information, Table SI-1) we depicted the different phases we observed on the X-Ray patterns: NSβ' for nanoscrolls with lipids in gel phase (β' indicates that the aliphatic chains are tilted), NSα for nanoscrolls with lipids in fluid phase and NT for nanotubes. The interaction of lanreotide with DMPC/DMPA membranes induces a drastic decrease of the phase transition temperature (of about 20°C) until the saturation of membranes by the peptide, *i.e*. for R_q about 1.

Altogether, these results indicate that *i)* the peptide is self-assembled at the surface of lipid bilayers, *ii)* the peptide packing in this self-assembly is very similar to the peptide packing within the nanotube walls *iii)* this interaction decreases drastically the temperature of the gel to fluid phase transition of the lipids and *iv)* the mixed lipid-peptide lamellae spontaneously stack to form multilamellar and rolled up on themselves structures.

The indexation of the X-Ray pattern of DMPC/DMPA-lanreotide (30/70%; [lip]=26mM and lanreotide R_q 1.2) at 23.5°C and at 48.5°C was done by trial and error approach using an homemade program in order to find an unique set of unit cell parameters and an indexation for all the observed peaks. Lamellar peaks (00l) were first indexed. The 2D lattice (hk0) was then indexed with an unit cell close to the lanreotide nanotubes. Additional peaks require the formation of a 2x2 superlattice, doubling the in-plane parameters. The cell parameters were then optimized to reduce the mean squared error. As a result, the X-Ray patterns obtained at 23.5 and 48.5°C have been indexed in a 3-D triclinic and a monoclinic unit cell respectively. The parameters of these two 3-D cells are reported on Table 2 (the indexations of the patterns at 23.5°C and 48.5°C are detailed in Supplementary Information, Table SI-2).

At 23.5°C, the "c" parameter (67.2 Å) corresponds well to the lamellae interdistance measured by electron microscopy (Figure 3, 60±10Å). This distance (67.2Å) corresponds to a stacking of a lipid bilayer and of a peptide bilayer The cell parameters "a" (46.7 Å) and "b" (40.2 Å) (Table 2) represent the unit cell for the peptide packing. The surface delimited by "a" and "b" (1820 Å^2) is about 4.5 times higher than the 2-D unit cell of the peptide in the

nanotubes[2] (Figure 1 D, a=20.7Å and b=20.8Å, γ=119° and S=400Å^2)[2] indicating that instead of two molecules of peptide, 8 peptides can fit within the surface delimited by *a* and *b* parameters.

Table 2: Unit cell parameters at 23.5°C and 48.5°C of DMPC/DMPA-Lanreotide R_q =1.2

	a (Å)	b (Å)	c (Å)	α°	β°	γ°	Vol (Å^3)
23,5°C	46.7	40.2	67.2	94.9	90.3	93.7	125364.8
48,5°C	44.7	39.6	56.9	90	90	94.3	100495.4

If we consider that these objects are formed for electroneutrality conditions, 25 molecules of lipids should fit within this surface allowing the presence of 16 molecules of DMPA required for electroneutrality. This amount of lipids give an average surface/lipid of 79Å^2. The area we deduced from the analysis of the wide angle X-ray scattering pattern was in the same order of magnitude, *i.e.* 76Å^2 (supplementary information, Figure S1-4). These area values are significantly higher than for example 60 Å^2 determined for fully hydrated DMPC.[30] Therefore, the assembly of the peptide at the membrane surface induces strong constraints on the lipid organization that increases of the average surface occupied by the lipid. This observation very well explains the decrease of the transition temperature as well as the 40° angle of the aliphatic chain when lipids are in the gel phase. Using these structural information, we built a molecular model (Figure 7). We show, that the interaction between lanreotide and anionic membrane, induces the formation of multilamellar structures, *i.e.* nanoscrolls, the curvature radius of the lamellae continuously varying within the same object. The resulting nanoscrolls are formed by alternate peptide and lipid bilayers in strong electrostatic interaction. The structural and spectroscopic data also indicate that the molecular packing of lanreotide within the nanotubes and within the nanoscrolls are very similar. The most important change is the surface of the unit cell that is four times higher than in the nanotubes.

For the pure lanreotide architectures, *i.e.* nanotubes, we have previously shown that curvature radius of the nanotube is due to the difference of the peptide packing on the two layers forming the nanotube wall[2]. We have also shown that the strictly uniform diameter of the nanotubes is controlled by close contacts between the lateral chains within the assembly[31] or by the size of the counterions[24]. Finally, in presence of divalent counterions, double walled nanotubes are formed but never multi walled nanotubes because the adhesion energy coming from the divalent anions that counterbalances the mechanic rigidity of the crystalline wall was too low[25]. Therefore, within the nanoscrolls,

the doubling in each direction *a* and *b* should be due to a double ripple surface of the architecture. This double ripple surface cannot be observed by our electron microscopy due to the low resolution.

CONCLUSIONS

The nanoscrolls that we observed in this study remarkably look like the ones observed when Ca^{2+} interacts with negatively charges lipids such as phosphatidylserine or phosphatidylglycerol. In these studies, the interaction between lipids and Ca^{2+}, besides the formation of nanoscrolls, induces a drastic increase of the gel to liquid phase transition temperature of the lipids as seen by differential scanning calorimetry. Moreover, the authors also showed that the nanoscroll structures disappeared upon the addition of ethylene diamine tetra acetic acid (EDTA), a strong chelating agent for Ca^{2+}. It is proposed that Ca^{2+} induces a flip-flop of the negatively charged lipids, creating an asymmetric membrane[32]. In both cases, lanreotide and Ca^{2+}, the interaction is driven by strong electrostatic attraction. However, in our case, lanreotide decreases the gel-liquid phase transition as seen by X-Ray scattering. As the peptide self-assembles at the surface of the membrane, one possibility is that the strong electrostatic interaction between the lipids and the peptide crystalline self-assembly induces a reorganization of the lipid packing.

Another analogy between the mixed peptide-membrane studied in this work can be made with the myelin sheath. The intracytoplasmic proteins that are directly involved in the tight membrane packing are positively charged and the driving force for the membrane packing within the myelin is essentially electrostatic.[33,34] In particular, stacking of lipid membranes can be induced in vitro by the interaction of P2 basic proteins, one of the two major proteins involved in the myelin sheath structure[35]. More recently, septin, an ubiquitous protein regarded as one of cytoskeleton proteins, was shown not only to interact with clusters of negatively charged lipids, but also to self-assemble into filament when interacting with membranes either in vivo[36] or in vitro[37]. Lanreotide-negatively charge lipid membrane assemblies mimic well natural protein-membrane assemblies that have structural functions for the cells.

MATERIAL AND METHODS

MATERIAL

Lanreotide is provided by IPSEN. The lipids (ePC; ePA, DMPC, DMPA) are purchased from AVANTI Polar Lipids and used without any further purification. The ultrafiltration units (AMICON centrifugal filter units) of 0.5ml are used, quartz capillaries, DMSO

METHODS

Small unilamellar liposomes

The lipids are dissolved in chloroform: methanol (90:10 v/v) and then evaporated using a Büchi Rotavapor R-200 for obtaining a thin and homogeneous film. The film is then hydrated with a precise volume of pure water and the lipid solution is vigorously vortexed. This solution is dispatched in different small vials that have been previously weighted. The samples are then frozen and lyophilized overnight. After lyophilization, each vials containing lipids are weighted to estimate the quantity of lipids. The lyophilized lipids are then hydrated and rigorously vortexted. For natural lipids, the suspensions, kept in ice, are then submitted to 10 cycles of 1min sonication followed by 3 min without sonication. For synthetic lipids such as DMPC and DMPA the lipid suspensions are kept at room temperature. When liposomes are prepared for ultrafiltration experiments, 0.1% (M/M) of Laurdan, a lipid fluorescence probe, is added to the lipids allowing the quantification of lipids.

Liposomes-lanreotide mixtures

The unilamellar vesicles are mixed with the appropriate lanreotide solution and rigorously vortexed. The samples are kept one day before ultrafiltration experiment to allow equilibration. When synthetic lipid mixtures such as DMPC/DMPA are used, the sample are subjected to 10 annealing cycles between 40°C and 5°C to accelerate equilibration.

Ultrafiltration experiments

In order to find the most convenient ultrafiltration unit for our experiments, we tested different cut-off (between 3KD and 100KD) and two different filtration membranes (polyethersulfone and cellulose). Lanreotide forms nanotubes when the total peptide concentration exceeds 17mM, *i.e.* its critical self-assembly concentration (CAC). [21] After spinning a solution of 41mM using the different ultrafiltration units, only the Amicon® Ultra, 0.5ml (cellulose membrane and 50KD cut-off) gave a satisfactory result (Supplementary Information, Figure SI-5), *i.e*. a concentration of lanreotide in the filtrate corresponding to its critical assembly concentration.

The experiments were performed as follow: 0.4ml of each sample is pipetted in the filter unit and is subjected to either 14000rpm during 10min or 5000 rpm during half an hour. The UV spectra of the solutions in the resulting

filtrate are recorded on a UV-Visible spectrophotometer (GE Healthcare, Ultrospec7000). The concentration of lanreotide in the filtrate is calculated from the optical density at 280nm using the molar absorption coefficient determined previously at 12000 $M^{-1}.cm^{-1}$ and compared to the initial lanreotide concentration in the samples. For the measurement of lanreotide within the samples containing lipids and to avoid errors due to light scattering, the initial solution are dissolved in DMSO.

Sample preparation for electron microscopy

Electron microscopy is performed on the samples either after negative staining or freeze-fracture for visualizing the object formed by lanreotide and lipids. For negative staining, we used uranyl acetate 1% as previously described[23]. For freeze fracture, we used a Balzers (BAF 600) apparatus. Different techniques has been used depending on the sample and the information we wanted to reach: simple Pt (30°) carbon replica after surface fracturing, Pt (30°) carbon replica obtained after surface fracturing and etching or rotative Pt pulverization and carbon replica after fracturing and etching.

Small angle X-Ray scattering

SAXS was performed on the high brilliance SWING beam line (12 KeV) at the Soleil Synchrotron Facility using sample-detector distances of 0.5m. The diffraction patterns were recorded for reciprocal spacing q ($Å^{-1}$) from 0.02 to 1.8 $Å^{-1}$. The X-ray patterns were detected and recorded via a chip charge-coupled device camera detector, AVIEX. The samples were prepared in 1.1 to 1.5mm glass capillaries (Glas Technik and Konstruktion, Schönewalde, Germany) and introduced into a homemade capillary holder accommodating 20 capillaries at controlled temperature. For each capillary, 34 patterns (exposure time 50 msec) were recorded from the top to the bottom to test homogeneity of the sample and to avoid degradation during measurements. All samples exhibited powder diffraction and scattering intensities as a function of the radial wave vector q ($q=4\pi*\sin(\theta)/\lambda$) which was determined by circular integration. The diffraction spacing were calibrated using the lamellar peaks of silver behenate (d = 53.380 Å).

For temperature scanning experiments, the samples were heated directly in the homemade capillary holder connected to a programmable thermostatic bath. The heating rate was fixed 0.16°C/min leading to an average difference of 3°C between each recorded X-Ray patterns of the same sample.

ATR-FTIR spectroscopy

Attenuated total reflectance Fourier transform infrared spectroscopy (ATR-FTIR) spectra were measured at 4 cm^{-1} resolution with a Bruker IFS 66 spectrophotometer equipped with a 45° n ZnSe ATR attachment. The spectra shown resulted from the average of 50 scans. Spectra were corrected for the linear dependence on the wavelength of the absorption measured by ATR. The water signal was removed by subtraction of a pure water spectrum recorded the day of the experiment. Analysis of the lanreotide conformation was performed by decomposition of the absorption spectra using GRAMS software, as a sum of Gaussian-Lorentzian (10%) components[38].

ASSOCIATED CONTENT

The supporting information file (pdf) is available free of charge. Additional material includes electron micrographs of ePC-lanreotide solution after ultrafiltration, fit of the inside structure of nanoscrolls with Archimedean spiral, X-ray patterns of DMPC/DMPA (30/70% m/M)-lanreotide R_q>1.2, wide angle X-ray analysis and the indexation tables of the patterns at 23.5°C and 48.5°C of DMPC/DMPA(30/70% m/M)-lanreotide R_q=1.2.

AUTHOR INFORMATION

Corresponding Author :* maite.paternostre@i2bc.paris-saclay.fr

Present Addresses

†Joel Richard MedinCell, Jacou, Languedoc-Roussillon, France

Author Contributions

All authors have given approval to the final version of the manuscript.

Funding Sources

This work has been realized in the context of ArchiPex, a joint laboratory between Industry (Beaufour Ipsen Industry) and two academic teams belonging to the institute of physics of Rennes (IPR) and the Institute for Integrative Biology of the Cell (I2BC) respectively.

ACKNOWLEDGMENT

We are thankful to the ANR program "ANR-LabCom" for funding the research of Archi-Pex (Project N°ANR-14-LAB5-0001-001). We sincerely acknowledge the TEM Team of Joliot Institute and the Biophysics platform of I2BC supported by French Infrastructure for Integrated Structural Biology (FRISBI) ANR-10-INBS-05. Drs Sonia Fieulaine, Yves Boulard and Stéphane Bressanelli are warmly thanked for advises and scientific discussions.

ABBREVIATIONS

CAC: critical self-assembly concentration; ePC: egg- phosphatidylcholine; ePA: egg-phosphatidic acid; DMPC: di-myristoylphosphatidylcholine; DMPA: di-myristoylphosphatidic acid; ATR-FTIR: attenuated total reflectance Fourier transformed infrared spectroscopy; R_q; charge ratio between the cationic charges and the anionic charges; NS: Nanoscrolls; NT: Nanotubes.

REFERENCES

(1) Subramanian, G.; Hjelm, R. P.; Deming, T. J.; Smith, G. S.; Li, Y.; Safinya, C. R. Structure of Complexes of Cationic Lipids and Poly(Glutamic Acid) Polypeptides: A Pinched Lamellar Phase. *J. Am. Chem. Soc.* **2000**, *122* (1), 26–34. https://doi.org/10.1021/ja991905j.

(2) Valery, C.; Paternostre, M.; Robert, B.; Gulik-Krzywicki, T.; Narayanan, T.; Dedieu, J. C.; Keller, G.; Torres, M. L.; Cherif-Cheikh, R.; Calvo, P.; et al. Biomimetic Organization: Octapeptide Self-Assembly into Nanotubes of Viral Capsid-like Dimension. *Proc. Natl. Acad. Sci. U. S. A.* **2003**, *100* (18), 10258–10262. https://doi.org/10.1073/pnas.1730609100.

(3) Valery, C.; Deville-Foillard, S.; Lefebvre, C.; Taberner, N.; Legrand, P.; Meneau, F.; Meriadec, C.; Delvaux, C.; Bizien, T.; Kasotakis, E.; et al. Atomic View of the Histidine Environment Stabilizing Higher-PH Conformations of PH-Dependent Proteins. *Nat. Commun.* **2015**, *6*, 7771. https://doi.org/10.1038/ncomms8771.

(4) Valery, C.; Artzner, F.; Paternostre, M. Peptide Nanotubes: Molecular Organisations, Self-Assembly Mechanisms and Applications. *Soft Matter* **2011**, *7* (20), 9583–9594. https://doi.org/10.1039/c1sm05698k.

(5) Sasso, L.; Suei, S.; Domigan, L.; Healy, J.; Nock, V.; Williams, M. a. K.; Gerrard, J. A. Versatile Multi-Functionalization of Protein Nanofibrils for Biosensor Applications. *Nanoscale* **2014**, *6* (3), 1629–1634. https://doi.org/10.1039/C3NR05752F.

(6) Wei, G.; Su, Z.; Reynolds, N. P.; Arosio, P.; Hamley, I. W.; Gazit, E.; Mezzenga, R. Self-Assembling Peptide and Protein Amyloids: From Structure to Tailored Function in Nanotechnology. *Chem. Soc. Rev.* **2017**, *46* (15), 4661–4708. https://doi.org/10.1039/C6CS00542J.

(7) Hughes, S. A.; Wang, F.; Wang, S.; Kreutzberger, M. A. B.; Osinski, T.; Orlova, A.; Wall, J. S.; Zuo, X.; Egelman, E. H.; Conticello, V. P. Ambidextrous Helical Nanotubes from Self-Assembly of Designed Helical Hairpin Motifs. *Proc. Natl. Acad. Sci.* **2019**, 201903910. https://doi.org/10.1073/pnas.1903910116.

(8) Baker, E. G.; Bartlett, G. J.; Porter Goff, K. L.; Woolfson, D. N. Miniprotein Design: Past, Present, and Prospects. *Acc. Chem. Res.* **2017**, *50* (9), 2085–2092. https://doi.org/10.1021/acs.accounts.7b00186.

(9) Silk, M. R.; Mohanty, B.; Sampson, J. B.; Scanlon, M. J.; Thompson, P. E.; Chalmers, D. K. Controlled Construction of Cyclic d / l Peptide Nanorods. *Angew. Chem.-Int. Ed.* **2019**, *58* (2), 596–601. https://doi.org/10.1002/anie.201811910.

(10) Jucker, M.; Walker, L. C. Self-Propagation of Pathogenic Protein Aggregates in Neurodegenerative Diseases. *Nature* **2013**, *501* (7465), 45–51. https://doi.org/10.1038/nature12481.

(11) Blancas-Mejía, L. M.; Ramirez-Alvarado, M. Systemic Amyloidoses. *Annu. Rev. Biochem.* **2013**, *82* (1), 745–774. https://doi.org/10.1146/annurev-biochem-072611-130030.

(12) Akinlolu, R. D.; Nam, M.; Qiang, W. Competition between Fibrillation and Induction of Vesicle Fusion for the Membrane-Associated 40-Residue Beta-Amyloid Peptides. *Biochemistry* **2015**, *54* (22), 3416–3419. https://doi.org/10.1021/acs.biochem.5b00321.

(13) Spillantini, M. G.; Schmidt, M. L.; Lee, V. M.-Y.; Trojanowski, J. Q.; Jakes, R.; Goedert, M. α-Synuclein in Lewy Bodies. *Nature* **1997**, *388* (6645), 839–840. https://doi.org/10.1038/42166.

(14) Burré, J.; Sharma, M.; Tsetsenis, T.; Buchman, V.; Etherton, M. R.; Südhof, T. C. α-Synuclein Promotes SNARE-Complex Assembly in Vivo and in Vitro. *Science* **2010**, *329* (5999), 1663–1667. https://doi.org/10.1126/science.1195227.

(15) Liang, H.; Angelini, T. E.; Ho, J.; Braun, P. V.; Wong, G. C. L. Molecular Imprinting of Biomineralized CdS Nanostructures: Crystallographic Control Using Self-Assembled DNA−Membrane Templates. *J. Am. Chem. Soc.* **2003**, *125* (39), 11786–11787. https://doi.org/10.1021/ja036529o.

(16) Liang, H.; Angelini, T. E.; Braun, P. V.; Wong, G. C. L. Roles of Anionic and Cationic Template Components in Biomineralization of CdS Nanorods Using Self-Assembled DNA−Membrane Complexes. *J. Am. Chem. Soc.* **2004**, *126* (43), 14157–14165. https://doi.org/10.1021/ja046718m.

(17) Henry, E.; Dif, A.; Schmutz, M.; Legoff, L.; Amblard, F.; Marchi-Artzner, V.; Artzner, F. Crystallization of Fluorescent Quantum Dots within a Three-Dimensional Bio-Organic Template of Actin Filaments and Lipid Membranes. *Nano Lett.* **2011**, *11* (12), 5443–5448. https://doi.org/10.1021/nl203216q.

(18) Liu, J.; Song, B.; Li, J.; Tian, X.; Ma, Y.; Yang, K.; Yuan, B. Photoluminescence Modulation of Silicon Nanoparticles via Highly Ordered Arrangement with Phospholipid Membranes. *Colloids Surf. B Biointerfaces* **2018**, *170*, 656–662. https://doi.org/10.1016/j.colsurfb.2018.06.066.

(19) Van Grondelle, W.; Iglesias, C. L.; Coll, E.; Artzner, F.; Paternostre, M.; Lacombe, F.; Cardus, M.; Martinez, G.; Montes, M.; Cherif-Cheikh, R.; et al. Spontaneous Fibrillation of the Native Neuropeptide Hormone Somatostatin-14. *J. Struct. Biol.* **2007**, *160* (2), 211–223. https://doi.org/10.1016/j.jsb.2007.08.006.

(20) van Grondelle, W.; Lecomte, S.; Lopez-Iglesias, C.; Manero, J.-M.; Cherif-Cheikh, R.; Paternostre, M.; Valery, C. Lamination and Spherulite-like Compaction of a Hormone's Native Amyloid-like Nanofibrils: Spectroscopic Insights into Key Interactions. *Faraday Discuss.* **2013**, *166*, 163–180. https://doi.org/10.1039/c3fd00054k.

(21) Valery, C.; Artzner, F.; Robert, B.; Gulick, T.; Keller, G.; Grabielle-Madelmont, C.; Torres, M. L.; Cherif-Cheik, R.; Paternostre, M. Self-Association Process of a Peptide in Solution: From Beta-Sheet Filaments to Large Embedded Nanotubes. *Biophys. J.* **2004**, *86* (4), 2484–2501.

(22) Valery, C.; Pouget, E.; Pandit, A.; Verbavatz, J.-M.; Bordes, L.; Boisde, I.; Cherif-Cheikh, R.; Artzner, F.; Paternostre, M. Molecular Origin of the Self-Assembly of Lanreotide into Nanotubes: A Mutational Approach. *Biophys. J.* **2008**, *94* (5), 1782–1795. https://doi.org/10.1529/biophysj.107.108175.

(23) Pouget, E.; Fay, N.; Dujardin, E.; Jamin, N.; Berthault, P.; Perrin, L.; Pandit, A.; Rose, T.; Valery, C.; Thomas, D.; et al. Elucidation of the Self-Assembly Pathway of Lanreotide Octapeptide into Beta-Sheet Nanotubes: Role of Two Stable Intermediates. *J. Am. Chem. Soc.* **2010**, *132* (12), 4230–4241. https://doi.org/10.1021/ja9088023.

(24) Gobeaux, F.; Fay, N.; Tarabout, C.; Meriadec, C.; Meneau, F.; Ligeti, M.; Buisson, D.-A.; Cintrat, J.-C.; Nguyen, K. M. H.; Perrin, L.; et al. Structural Role of Counterions Adsorbed on Self-Assembled Peptide Nanotubes. *J. Am. Chem. Soc.* **2012**, *134* (1), 723–733. https://doi.org/10.1021/ja210299g.

(25) Gobeaux, F.; Fay, N.; Tarabout, C.; Meneau, F.; Meriadec, C.; Delvaux, C.; Cintrat, J.-C.; Valery, C.; Artzner, F.; Paternostre, M. Experimental Observation of Double-Walled Peptide Nanotubes and Monodispersity Modeling of the Number of Walls. *Langmuir* **2013**, *29* (8), 2739–2745. https://doi.org/10.1021/la304862f.

(26) Krimm, S.; Bandekar, J. Vibrational Spectroscopy and Conformation of Peptides, Polypeptides, and Proteins. In *Advances in Protein Chemistry*; Anfinsen, C. B., Edsall, J. T., Richards, F. M., Eds.; Academic Press, 1986; Vol. 38, pp 181–364. https://doi.org/10.1016/S0065-3233(08)60528-8.

(27) Barth, A. The Infrared Absorption of Amino Acid Side Chains. *Prog. Biophys. Mol. Biol.* **2000**, *74* (3), 141–173. https://doi.org/10.1016/S0079-6107(00)00021-3.

(28) Mantsch, H. H.; McElhaney, R. N. Phospholipid Phase Transitions in Model and Biological Membranes as Studied by Infrared Spectroscopy. *Chem. Phys. Lipids* **1991**, *57* (2), 213–226. https://doi.org/10.1016/0009-3084(91)90077-O.

(29) Garidel, P.; Johann, C.; Blume, A. Nonideal Mixing and Phase Separation in Phosphatidylcholine Phosphatidic Acid Mixtures as a Function of Acyl Chain Length and PH. *Biophys. J.* **1997**, *72* (5), 2196–2210.

(30) Kučerka, N.; Liu, Y.; Chu, N.; Petrache, H. I.; Tristram-Nagle, S.; Nagle, J. F. Structure of Fully Hydrated Fluid Phase DMPC and DLPC Lipid Bilayers Using X-Ray Scattering from Oriented Multilamellar Arrays and from Unilamellar Vesicles. *Biophys. J.* **2005**, *88* (4), 2626–2637. https://doi.org/10.1529/biophysj.104.056606.

(31) Tarabout, C.; Roux, S.; Gobeaux, F.; Fay, N.; Pouget, E.; Meriadec, C.; Ligeti, M.; Thomas, D.; Ijsselstijn, M.; Besselievre, F.; et al. Control of Peptide Nanotube Diameter by Chemical Modifications of an Aromatic Residue Involved in a Single Close Contact. *Proc. Natl. Acad. Sci. U. S. A.* **2011**, *108* (19), 7679–7684. https://doi.org/10.1073/pnas.1017343108.

(32) Papahadjopoulos, D.; Ohki, S. Stability of Asymmetric Phospholipid Membranes. *Science* **1969**, *164* (3883), 1075–1077. https://doi.org/10.1126/science.164.3883.1075.

(33) Omlin, F. X.; Webster, H. D.; Palkovits, C. G.; Cohen, S. R. Immunocytochemical Localization of Basic Protein in Major Dense Line Regions of Central and Peripheral Myelin. *J. Cell Biol.* **1982**, *95* (1), 242–248. https://doi.org/10.1083/jcb.95.1.242.

(34) Inouye, H.; Kirschner, D. A. Evolution of Myelin Ultrastructure and the Major Structural Myelin Proteins. *Brain Res.* **2016**, *1641*, 43–63. https://doi.org/10.1016/j.brainres.2015.10.037.

(35) Sedzik, J.; Blaurock, A. E.; Hoechli, M. Reconstituted P2/Myelin-Lipid Multilayers. *J. Neurochem.* **1985**, *45* (3), 844–852. https://doi.org/10.1111/j.1471-4159.1985.tb04071.x.

(36) Caudron, F.; Barral, Y. Septins and the Lateral Compartmentalization of Eukaryotic Membranes. *Dev. Cell* **2009**, *16* (4), 493–506. https://doi.org/10.1016/j.devcel.2009.04.003.

(37) Bridges, A. A.; Zhang, H.; Mehta, S. B.; Occhipinti, P.; Tani, T.; Gladfelter, A. S. Septin Assemblies Form by Diffusion-Driven Annealing on Membranes. *Proc. Natl. Acad. Sci.* **2014**, *111* (6), 2146–2151. https://doi.org/10.1073/pnas.1314138111.

(38) Byler, D. M.; Susi, H. Examination of the Secondary Structure of Proteins by Deconvolved FTIR Spectra. *Biopolymers* **1986**, *25* (3), 469–487. https://doi.org/10.1002/bip.360250307.

(39) Zantl, R.; Baicu, L.; Artzner, F.; Sprenger, I.; Rapp, G.; Radler, J. O. Thermotropic Phase Behavior of Cationic Lipid-DNA Complexes Compared to Binary Lipid Mixtures. *J. Phys. Chem. B* **1999**, *103* (46), 10300–10310. https://doi.org/10.1021/jp991596j.

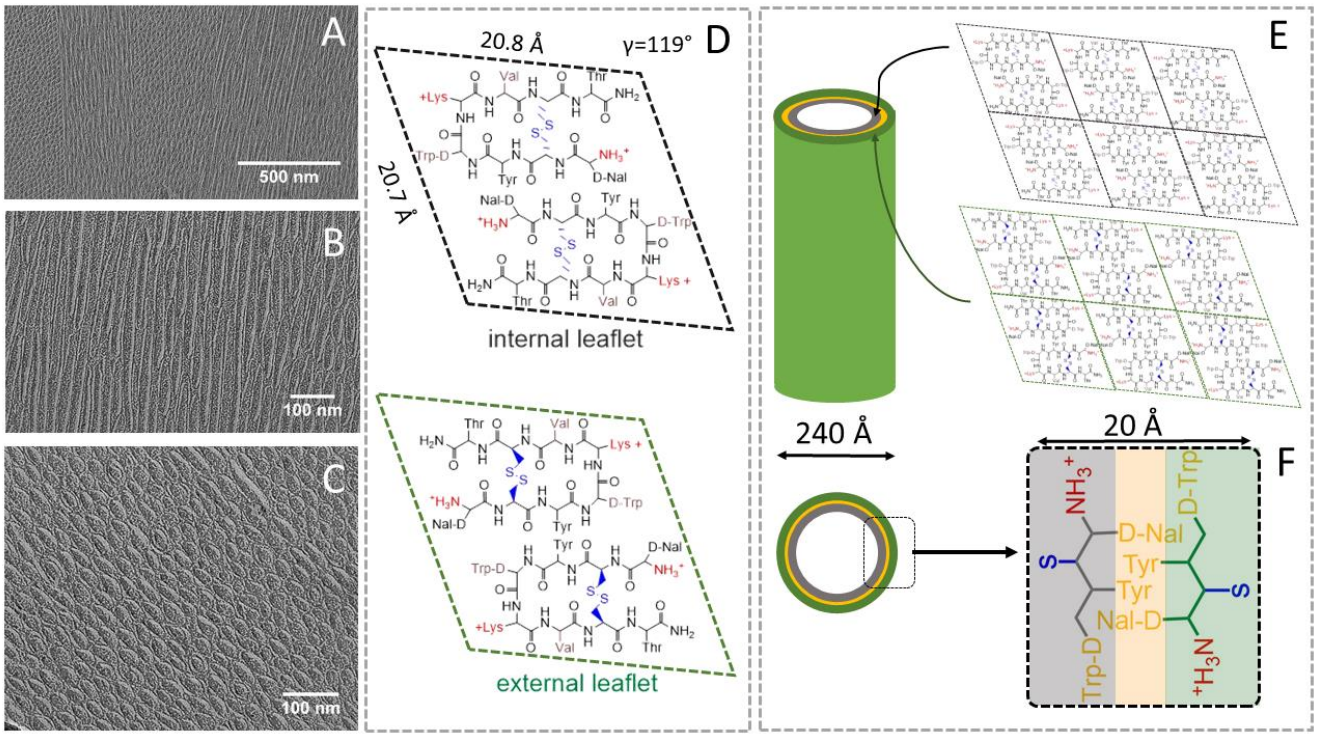

Figure 1: Morphology and structure of the nanotubes formed by the self-assembly of Lanreotide in water. Freeze-fracture micrographs of nanotubes that have been transversally and longitudinally cut (A) , zoom on longitudinally (B) and transversally (C) cut nanotubes. (D): Detail of the unit cell of the peptide crystal that form the wall of the nanotube. The two cationic charges of the peptide are indicated in red and are brought by the N-ter and the lysine residue. The wall is formed by a peptide bilayer and the two leaflets are not equivalent explaining the spontaneaous wall curvature. E: The nanotube structure and F: detail on the internal structure of the wall; the wall present two external hydrophilic surface and the hydrophobic residues (yellow) are concentrated within the wall at the interface between the internal and external leaflets (in grey and green respectively).

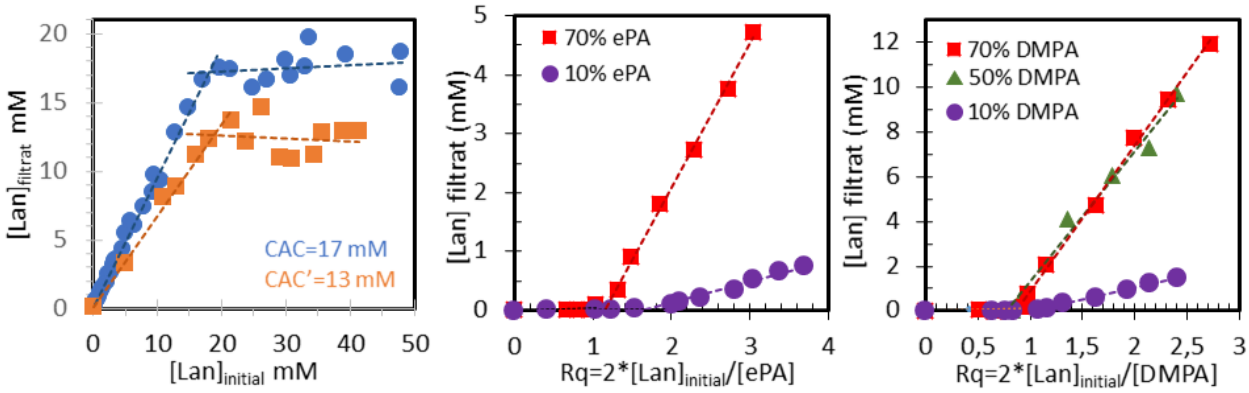

Figure 2: Ultrafiltration experiments of solutions containing Lanreotide (A, blue points) and solutions containing lanreotide and liposomes (A, orange points, B & C). For all the experiments in presence of lipids, we kept constant the total lipid concentration and increased the lanreotide one. (A) Evolution of the free lanreotide concentration measured in the filtrate with the initial lanreotide concentration in the solution (before ultrafiltration) for Lanreotide solutions (blue points) and for lanreotide-ePC liposomes (orange points) and [lip]=10mM. (B & C) Evolution of the lanreotide concentration in the filtrate with the charge ratio Rq (see text for definition), (B) Ultrafiltration of solutions containing Lanreotide & liposomes ([lip]=10mM) formed by either 90% of ePC and 10% of ePA (violet points) or 30% of ePC and 70% of ePA (red points). (C) Ultrafiltration of solutions containing Lanreotide & liposomes ([lip]tot=26mM) formed by 90% of DMPC and 10% of DMPA (violet points), 50% of DMPC and 50% of DMPA (green points), or 30% of ePC and 70% of ePA (red points). In all the samples containing lipids, the absence of lipid in the filtrate was controlled thanks to the fluorescent probe Laurdan (λexc=360nm; 360<λem<640nm) incorporated within the initial liposomes at 0.1% (M/M). The lipid concentration within the filtrate never exceeds 0,01 % of the initial lipid concentration.

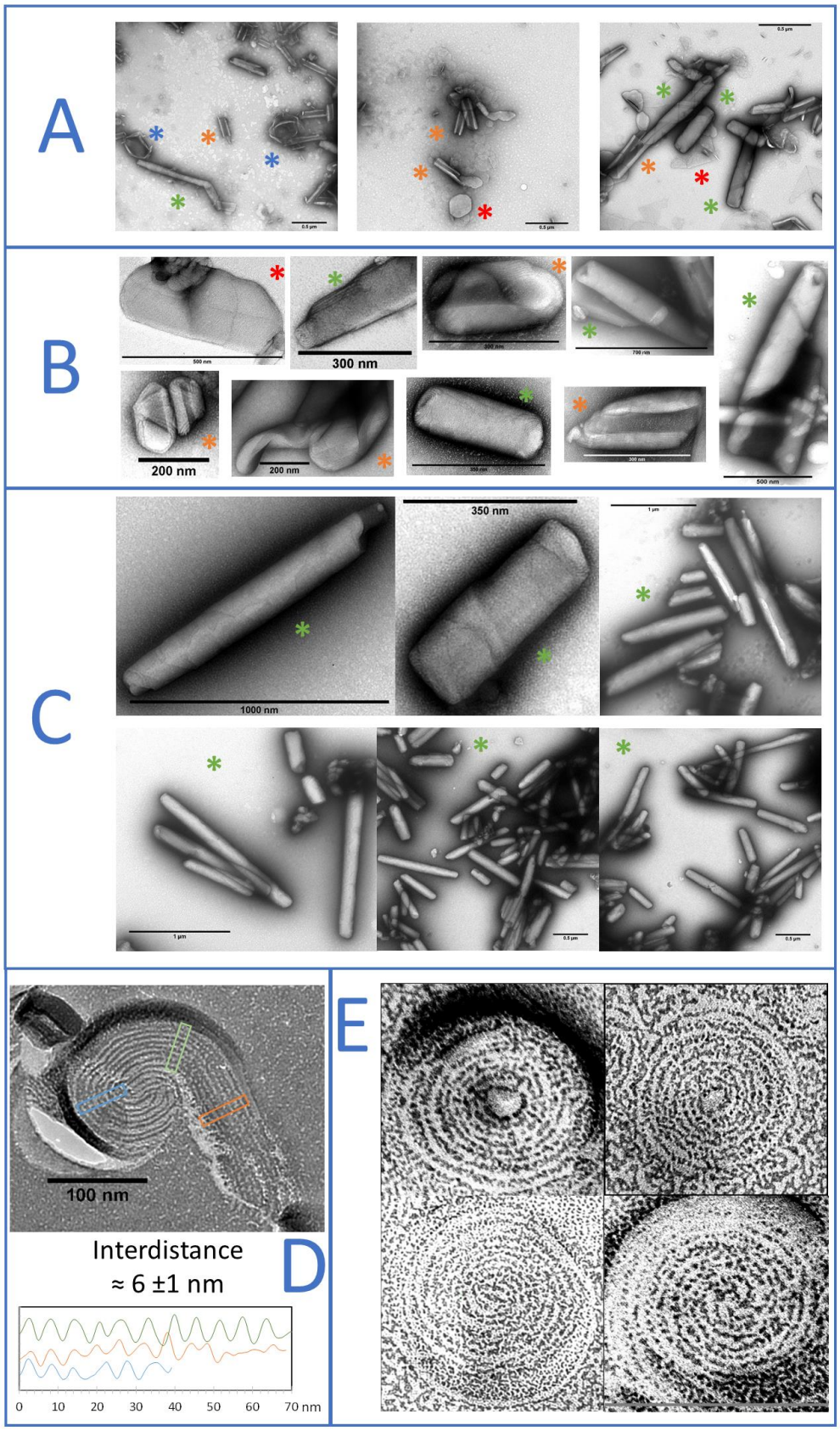
A
B
300 nm
200 nm
200 nm
C
350 nm
1000 nm
100 nm
Interdistance
≈ 6 ±1 nm
D
0
10
20
30
40
50
60
70 nm
E

Figure 3: Electron micrographs after negative staining of DMPC/DMPA(30/70% M/M)-lanreotide mixtures leading to Rq of 0.5 (A), 1 (B) and 2 (C) ([lip]=26mM). The stars on the micrographs indicate the different types of objects that are present within the sample: liposomes (blue star), planar lamellae (red star), curve stack of lamellae (orange star) and nanoscrolls (green star). D & E Electron micrographs after freeze fracture that reveals internal arrangement of the nanoscrolls. (D) Interdistance between lamellae determined from the blue, green and orange box and details of the spiral structure of the nanoscrolls (the micrographs have been taken for Rq =1).). The scales are indicated on each micrograph.

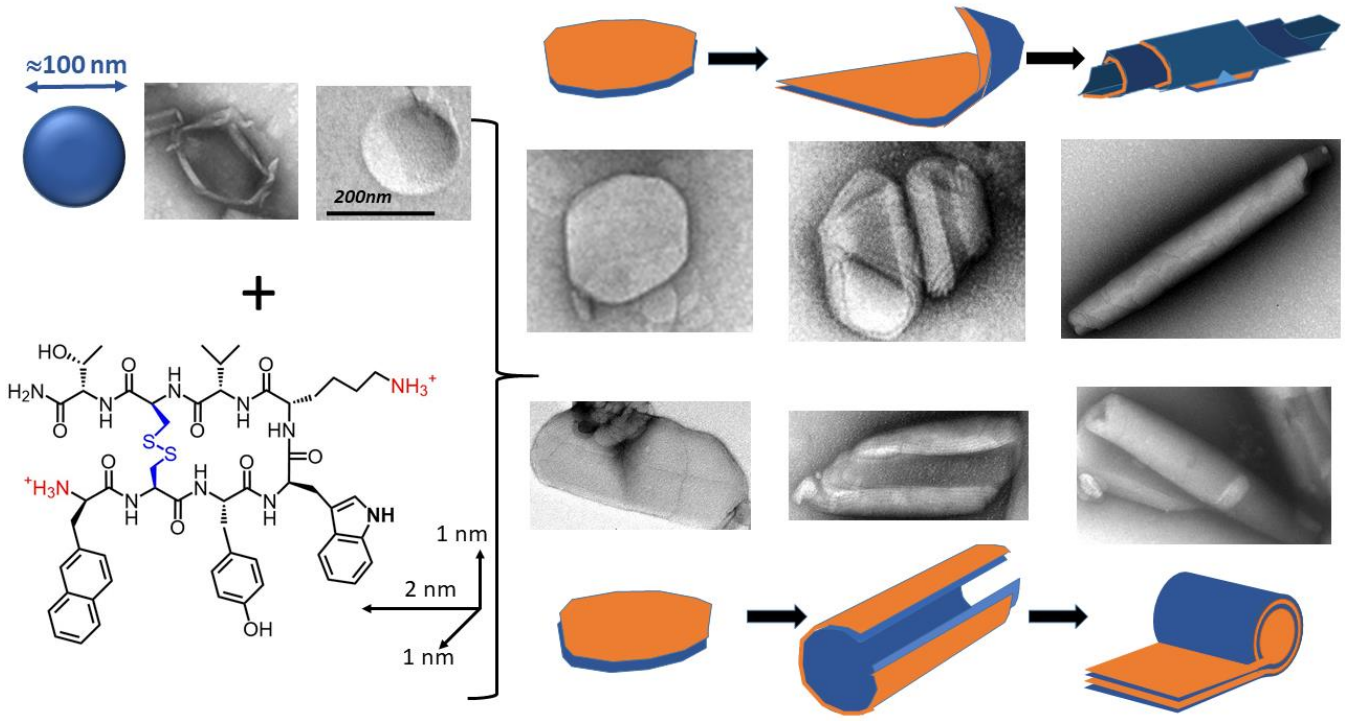

Figure 4: Steps of nanoscroll formation. Unilamellar liposomes of about 100nm (electron micrographs after negative staining and after freeze fracture) are mixed with lanreotide in monomeric state, the volume of which is about $2nm^3$. Upon interaction with the peptide, the liposomes disappear for planar lamellae that stack. These lamellae then curve forming uni- or multi-lamellae and finally form either diagonal nanoscrolls (upper scheme) or one-side nanoscrolls (lower scheme). The blue and orange sheets indicate that the structures are formed by the initial stacking of two different membranes composed of either lipids or peptides.

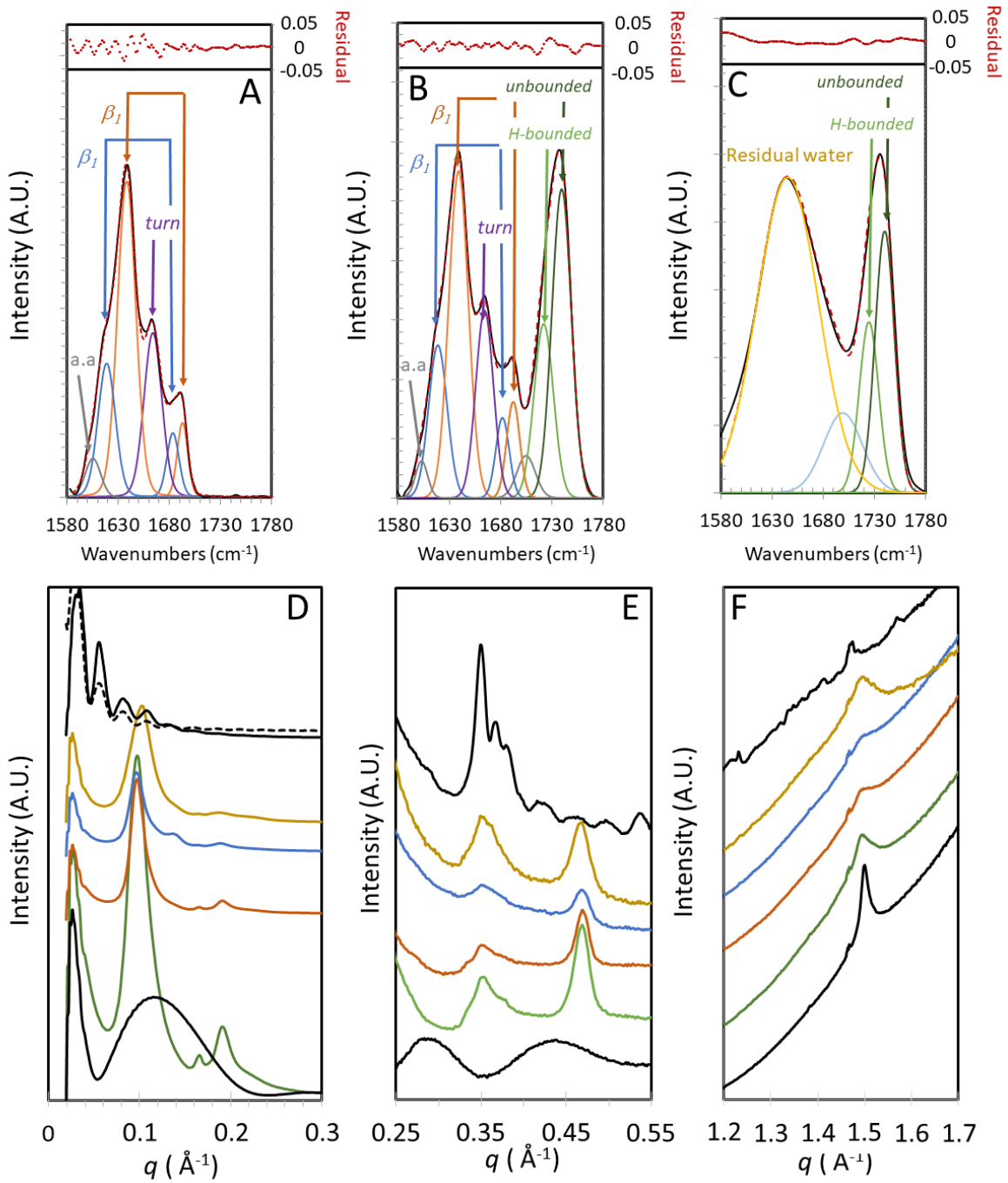

Figure 5: ATR-FTIR spectra (A, B & C) and X-ray scattering patterns (D, E & F). For ATR-FTIR spectra we focused on the Amide I band of the peptide backbone and the ester bond of the lipids (between 1580 and 1780cm-1). (A) ATR-FTIR spectrum of the Amide I band of nanotubes of peptide ([lan]=55.2mM); (B) ATR-FTIR spectrum of unilamellar vesicles of DMPC/DMPA (30/70% m/M-[lip]=158 mM) and lanreotide ([Lan]=55.2mM); (C) ATR-FTIR spectrum of the unilamellar vesicles of DMPC/DMPA (30/70% m/M and [lip]=158mM). For X-ray scattering patterns, we focused on three different regions of the patterns: (D) X-ray patterns between 0<q<0.3 Å-1 (small angles), (E) X-ray patterns between 0.25<q<0.55 Å-1 (intermediate angles) and (F) X-ray patterns between

1.2<q<1.7 Å-1 (wide angles). On each panel the same patterns are presented: black patterns: unilamellar vesicles of DMPC/DMPA (30/70% M/M-[lip]=26mM) (black lower traces) and peptide nanotubes ([Lan]=70mM) (back upper traces). The dotted black upper trace represents the fit of the peptide nanotubes by a Bessel function of zero order leading to a diameter of 238.5 Å. The other patterns were recorded for DMPC/DMPA (30-70% M/M and [lip]=26mM) containing increasing concentration of lanreotide to reach Rq =0.5 (green pattern), Rq =1 (orange pattern); Rq =1.6 (blue pattern) and Rq =2 (brown pattern).

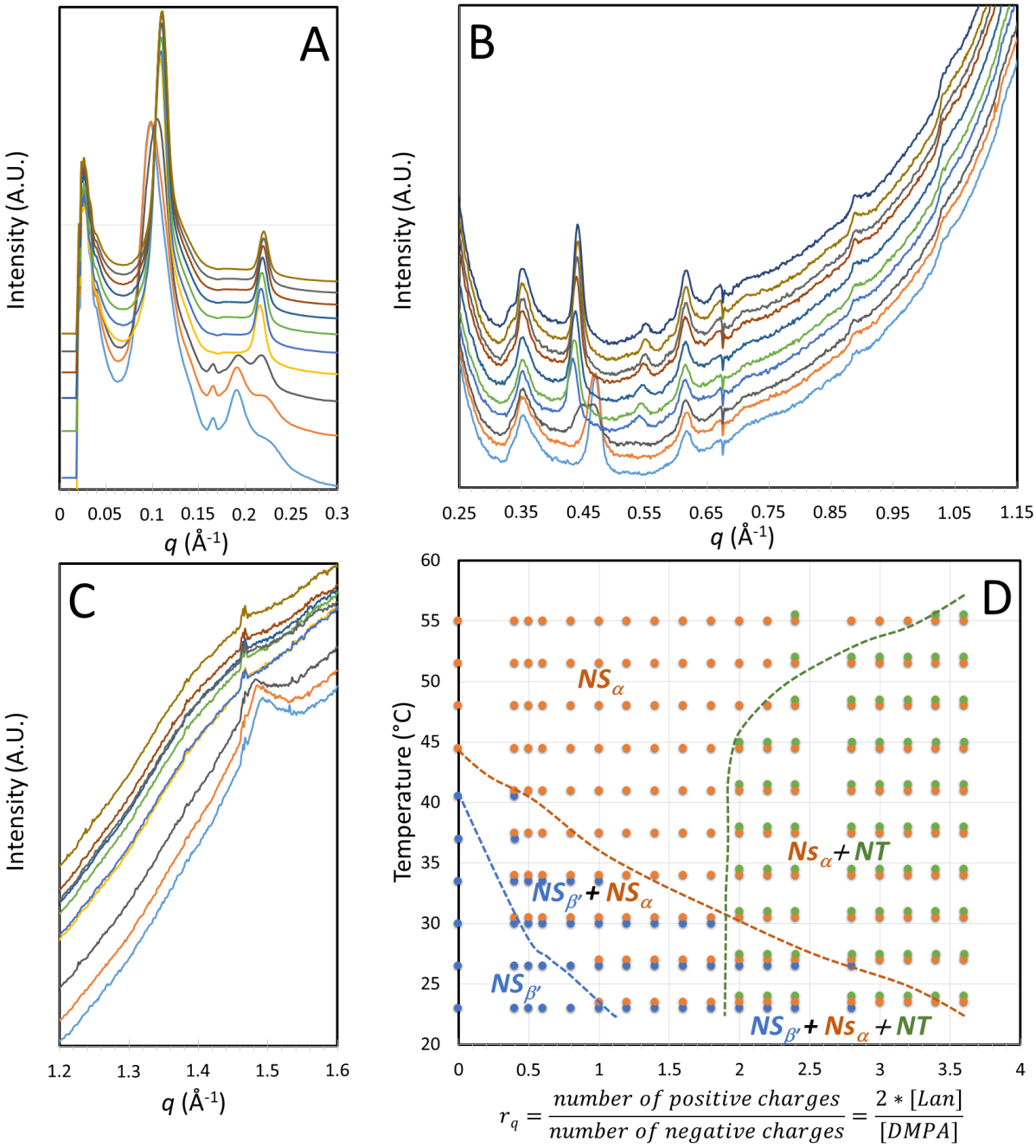

Figure 6: Evolution of the X-Ray patterns with temperature from 23.5°C to 55°C by increments of 3,5°C (from the bottom to the top) for DMPC/DMPA (30/70% M/M and [lip]=26mM)-Lanreotide Rq =1.2 (A, B & C) and phase diagram (D): blue points: lamellar stacking with lipids in Lβ phase, orange points: lamellar stacking with lipids in Lα phase and green points: peptide nanotubes.

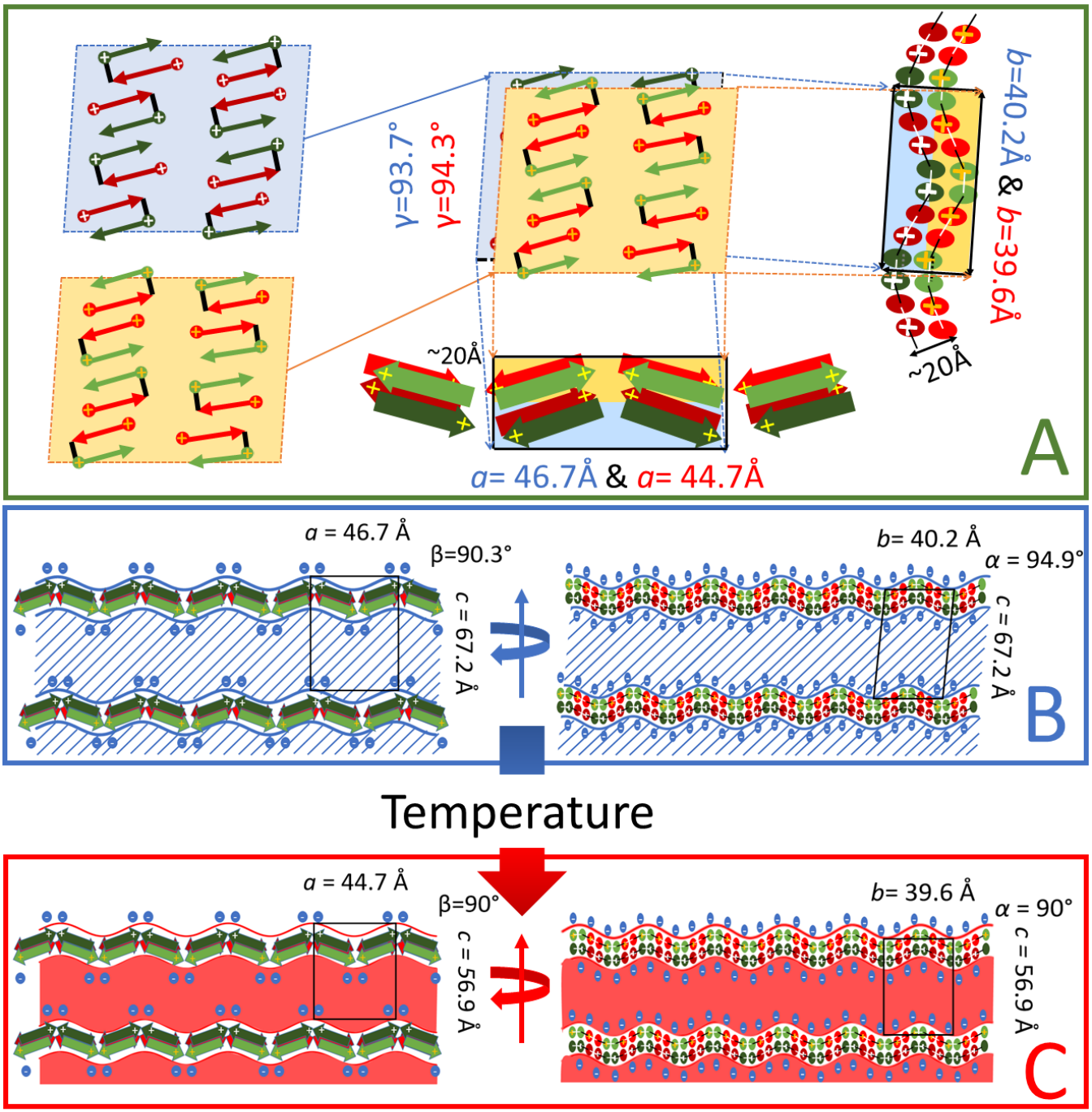

Figure 7: Molecular model of the nanoscrolls. Molecular packing of the peptide at the surface of the lipid bilayer (A), transversal views of the nanoscrolls structure for lipids in gel (B) and fluid (C) phase. Within panel B and C,

two 90° transversal views are schematized. (A) lanreotide molecule is schematized by a hairpin: the aromatic residues are located on the red branch of the hairpin and the aliphatic ones on the green branch. The positives charges of lanreotide are indicated in yellow. The peptide crystal is shown from the top. Two 90° transversal view of the peptide bilayer crystal are also described. The lipids are schematized in blue and in red when in the gel (B) or in the fluid (C) state.

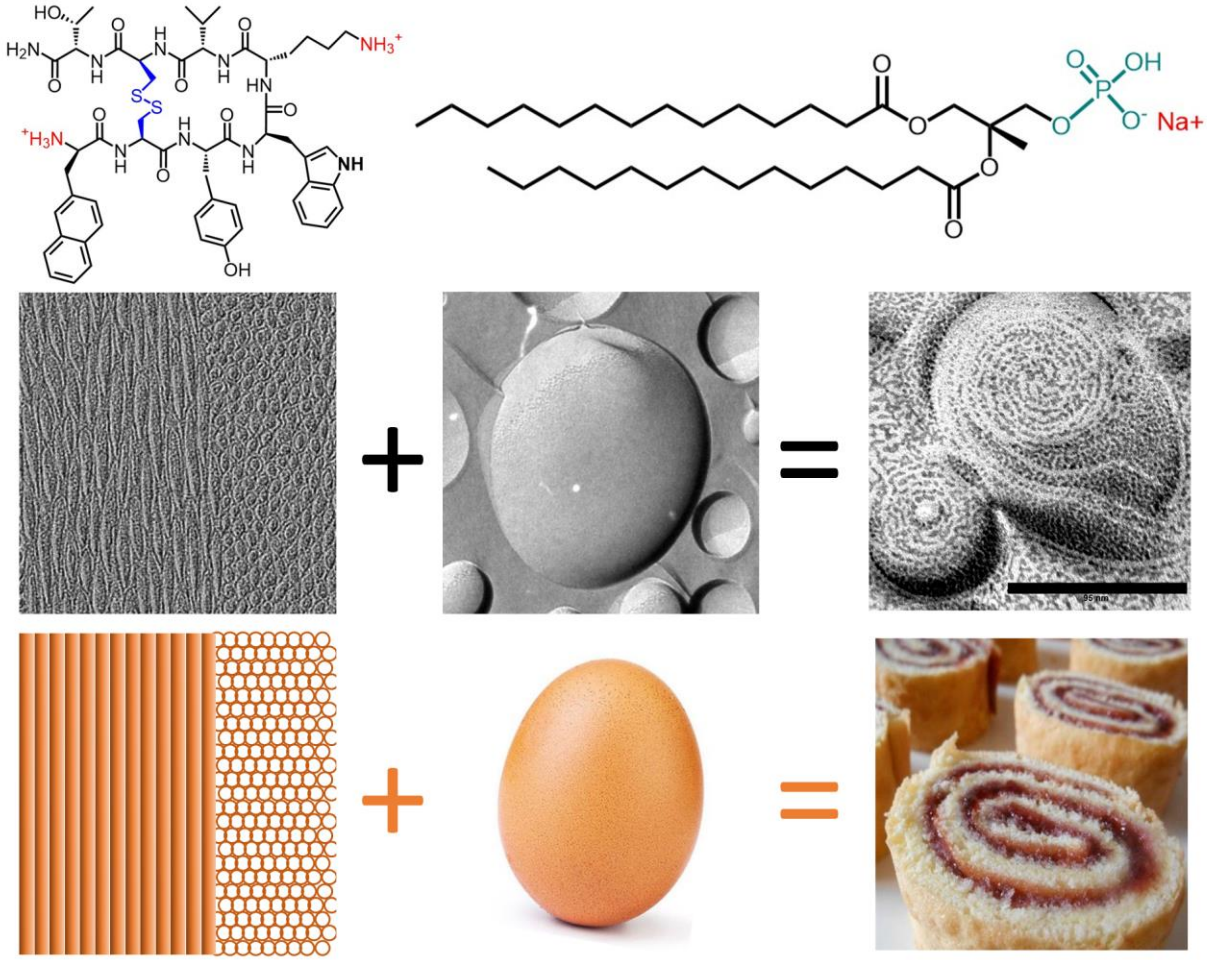
HO
H2N
NH3+
S-S
+H3N
NH
OH
O
OH
P
O-
Na+
+
=
+
=